Available online at www.sciencedirect.com
ScienceDirect
Control Engineering Practise 00 (2016) 1–18
Journal Logo

Nonlinear Observer Design for GNSS-Aided Inertial Navigation Systems with Time-Delayed GNSS Measurements

Jakob M. Hansen[1], Thor I. Fossen[1], Tor Arne Johansen[1]

Abstract

Global navigation satellite system (GNSS) receivers suffer from an internal time-delay of up to several hundred milliseconds leading to a degeneration of position accuracy in high-dynamic systems. With the increasing interest in GNSS navigation, handling of time-delays will be vital in high accuracy applications with high velocity and fast dynamics. This paper presents a nonlinear observer structure for estimating position, linear velocity, and attitude (PVA) as well as accelerometer and gyro biases, using inertial measurements and time-delayed GNSS measurements. The observer structure consists of four parts; a) attitude and gyro bias estimation, b) time-delayed translational motion observer estimating position and linear velocity, c) input delays for inertial and magnetometer measurements, and d) a faster than real-time simulator. The delayed PVA and gyro bias estimates are computed using a uniformly semiglobally exponentially stable (USGES) nonlinear observer. The high-rate inertial measurements are delayed and synchronized with the GNSS measurements in the state observer. The fast simulator integrates the inertial measurements from the delayed state estimate to provide a state estimate at current time. The sensor measurements are carefully synchronized and the estimation procedure for the GNSS receiver delay is discussed. Experimental data from a small aircraft are used to validate the results.

Keywords: Time-Delayed System, Inertial Navigation, Satellite Navigation Systems, GNSS-Aided Navigation

1. Introduction

Aiding an inertial navigation system (INS) with position and velocity updates from a Global Navigation Satellite System (GNSS) receiver is widely used for vehicle navigation. The inertial measurement unit (IMU) contributes with high sample rate linear acceleration and angular rate measurements, which are integrated to obtain position, velocity and attitude (PVA) estimates. However, the error builds up quickly resulting in poor accuracy for long-term predictions. The drift is compensated by using low sample rate GNSS measurements. The resulting system is a strapdown INS aided by GNSS measurements where the observer produces high sample rate state estimates.

The integration of inertial and GNSS measurements have traditionally been achieved using Kalman filters (KF) or extended Kalman filters (EKF) for nonlinear systems, see e.g. Grewal et al. [1]. Within the last decade another approach based on nonlinear observer design for estimating PVA is becoming increasingly popular. The design of nonlinear observers is grounded in systems theory where the stability properties are investigated. Thus the advantage of using nonlinear observers compared to EKFs is a significant reduction in computational load, guaranteed stability properties and reduced need for linearization of the system model. See e.g. Hua [2], Vik and Fossen [3], or Grip

Email address: jakob.mahler.hansen@itk.ntnu.no, thor.fossen@ntnu.no, tor.arne.johansen@itk.ntnu.no ()
[1]Department of Engineering Cybernetics, Norwegian University of Science and Technology, 7491 Trondheim, Norway.

et al. [4] for recent attention of nonlinear observers with significantly stronger stability results than nonlinear KFs. The reduction in computational load when using nonlinear observers compared to nonlinear KFs were investigated in Grip et al. [5] and Mahony et al. [6], and especially in Johansen et al. [7], where a tightly coupled nonlinear observer was shown to comprise less than 25% of the computational load of a multiplicative EKF (MEKF). The smaller computational footprint allows for a reduction in hardware requirements or increased availability of processing power for other applications. Recent work by Mahony et al. [6], Roberts and Tayebi [8], Hua et al. [9], and Kingston and Beard [10] as well as Grip et al. [11, 4, 5] use nonlinear observers to estimate PVA, acceleration bias, and gyro bias.

GNSS receivers experience a time delay due to the computational time for position estimation and the data communication time from the receiver to the user. The time delay can be disregarded for low-dynamic applications (e.g. marine vessels and pedestrian use), but it has great impact on high-dynamic systems such as high-precision automatic UAV and aircraft landing systems. For high-dynamic applications the sensor measurements should have high sample rate and accurate synchronization to minimize the estimation errors, Skog and Händel [12]. It is therefore important to identify and compensate for sensor time delays.

The work presented here aims to combine a nonlinear attitude observer with accurate position estimation taking the receiver time-delay into consideration. The paper is motivated by the increased interest in highly accurate GNSS applications. Due to the estimation inaccuracies introduced by time-delays in GNSS receivers it is believed time-delay compensation will be mandatory in future GNSS/INS applications with fast dynamics and high velocities.

Estimation in time-delayed systems have been subject to extensive research e.g. Jacovitti and Scarano [13] who investigated discrete-time systems. Latency determination and compensation are described by Solomon et al. [14] using an experimental setup. The approach of using Kalman filters for GNSS/IMU systems with time delay have been investigated by Raff and Allgöwer [15] and Skog and Händel [16]. Time synchronization errors in GNSS/IMU systems are discussed by Skog and Händel [12]. A Kalman filter handling delayed or asynchronous measurements is considered in Blanke [17, 18], where the focus is fault tolerant marine operations. Lyapunov functionals are used for stability analysis by Papachristodoulou et al. [19]. Stability of delayed systems is further investigated in Gu and Niculescu [20] and Albertos and Garcia [21]. Recently, a quadrotor helicopter application with time delays in the feedback loops was studied by Ailon and Arogeti [22]. In Battilotti [23] a class of nonlinear predictors for delayed measurements with a known and constant delay is proposed. The nonlinear observer consists of several couples of filters each estimating the state vector at some delayed time instant differing from the previous by a small fraction of the overall delay. By use of a small gain approach Ahmed-Ali et al. [24] presents a class of global exponential stable nonlinear observers with sampled and delayed measurements, robust towards measurement errors and sampling schedule perturbations. Also, Briat [25] and Fridman [26] present extensive research on stability and control of time-delayed systems, and Khosravian et al. [27, 28, 29] propose an observer-predictor approach to delayed GNSS and magnetometer measurements where current position is determined from delayed position estimates. In Siccardi et al. [30] timing issues in the pulse-per-second signals from GNSS receivers are investigated.

1.1. Contribution of the Paper

This paper presents a method for handling time-delayed GNSS measurement in a loosely-coupled strapdown GNSS/INS system. The observer structure is based on a USGES nonlinear PVA estimator, Grip et al. [5], where the high-rate inertial measurements are delayed to match the delayed GNSS measurements. A fast simulator uses inertial measurements to compensate for the delay in the state estimate. The main contribution is the modification and extension of the nonlinear observer to time-delayed position measurements. The observer makes a correction to the delayed state using the delayed GNSS measurement, which are integrated with delayed INS position estimates. The method can be generally applied to other GNSS/INS integration schemes that employ other state estimation algorithms. The presented approach is tested in a high-dynamic test environment using a small aircraft for experimental validation.

1.2. Organization of the Paper

The paper is organized as follows: Section 2 gives an introduction to the experienced time delay in GNSS receivers and how it can be estimated. Section 3 states the delayed navigation problem formally. Section 4 introduces the solution involving the nonlinear attitude estimator, the translational motion observer and the fast simulator. Section 5 presents an alternative implementation of the observer structure, while Section 6 presents simulation results. Section 7 contains experimental results using an unmanned aerial vehicle, while Section 8 gives the concluding remarks.

1.3. Notation and Preliminaries

A column vector $x \in \mathbb{R}$ is denoted $x := [x_1; x_2; x_3]$ with transpose $x^\intercal$ and vector norm $\|x\|_2$. The skew-symmetric matrix of a vector x is given as:

$$S(x) := \begin{bmatrix} 0 & -x_3 & x_2 \\ x_3 & 0 & -x_1 \\ -x_2 & x_1 & 0 \end{bmatrix}$$

The attitude can be described with a unit quaternion, $q = [r_q; s_q]$, consisting of a real part, $r_q \in \mathbb{R}$, and a vector part, $s_q \in \mathbb{R}^3$, where $\|q\|_2 = 1$. A vector $x \in \mathbb{R}^3$ can be expressed as a quaternion with zero real part; $\bar{x} = [0; x]$. The product between two quaternions q_1 and q_2 is determined with the Hamiltonian product denoted $q_1 \otimes q_2$.

Several coordinate frames will be utilized in the following where the superscripts e and b will denote the Earth-Centered-Earth-Fixed (ECEF) and the Body-fixed coordinate system, respectively. The local North-East-Down (NED) coordinate system will be denoted n while the Earth-Centered-Inertial frame is given by i. The rotation between two frames can be described using quaternions as, e.g. q_a^c, representing the rotation from generic coordinate frame a to frame c, with a corresponding rotation matrix $R(q_a^c) \in SO(3)$. The rotation of a vector x in the a frame to the c frame is then described as $R(q_a^c)x^a = x^c$ given by $R(q_a^c) = I + 2s_{q_a^c}S(r_{q_a^c}) + 2S(r_{q_a^c})^2$. Rotation rate will be denoted ω_{ac}^d representing the rotation of coordinate system c with respect to a decomposed in d. The Earth rotation rate ω_{ie}^e then describes the rotation of the ECEF frame in inertial frame decomposed in the ECEF frame, where $\omega_{ie}^e = [0, 0, 7.292115 \cdot 10^{-5}]\ rad/s$.

2. Time Delay of GNSS Receivers

Using GNSS measurements as aid in inertial navigation systems is widely used. However the inertial sensors commonly have a much (20–500 times) higher sample rate than the GNSS receiver. Accurate time stamping of the measurements in relation to each other is therefore vital in the effort to minimize the error, as falsely time stamped data will introduced errors: if the time of use does not correspond to the time of validity the vehicle might have moved or rotated in the time in-between. If one of the sensors in the aided system experiences a delay the integration precision will suffer as the measurements will not correspond to the correct time stamp.

It is widely known that the GNSS signal can experience delays when travelling from the satellites to the receiver (e.g. multipath, atmospheric delays, and timing errors between satellite and receiver clocks) but as the demand for increased accuracy of navigation solutions is growing, other delays will have to be taken into account as well. In the following the time delay arising between the time of validity of the satellite signals to the data is available to the user is considered. The time delay experienced in the GNSS receiver, stems from the computational time of the position estimation as well as the dissemination of the data from the receiver to the user. The total time delay is hence $\tau = \tau_{cal} + \tau_{dis}$, where the calculation time, τ_{cal}, depends on the number of satellites in the constellation, and the dissemination time, τ_{dis}, covers the time it takes the receiver to output the data to the user, which is directly dependent on the number of bytes to transmit and the communication protocol used. Ideally the position data should be available to the user exactly when the receiver obtains the satellite signals. However, even if the calculation of position could be done instantaneous the data would still be delayed with τ_{dis}.

To determine the delay, an accurate measure of the desired (without delay) time stamp is required: GNSS receivers often allow access to a pulse-per-second (PPS) signal, synchronized to satellite clock, indicating the arrival of new measurements. The PPS goes high when the GPS time is incremented with one second, leaving the PPS interval, as the time between two consecutive rising edges on the PPS signal, at one second. It is assumed that the PPS signal is not delayed in the receiver and can therefore be used as a reference for the ideal time-stamping of the GNSS measurements. The validity of the GNSS data can be related to such a pulse on the PPS signal, and it is therefore possible to directly measure the time delay by monitoring the edges on the PPS and data signals. Three edges are of interest: I) the rising edge of the PPS signal denoted as the time of validity (TOV), II) the first rising edge of the data signal denoting time of transmit (TOT) from the receiver to the user, and III) the time of arrival (TOA) defined as the final falling edge of the data-package. Here data packages are defined as sets of binary values sent on the data signal. The total time delay can then be estimated as the time between the TOV and TOA edges. The situation is visualized in Fig. 1, with example times for clarification.

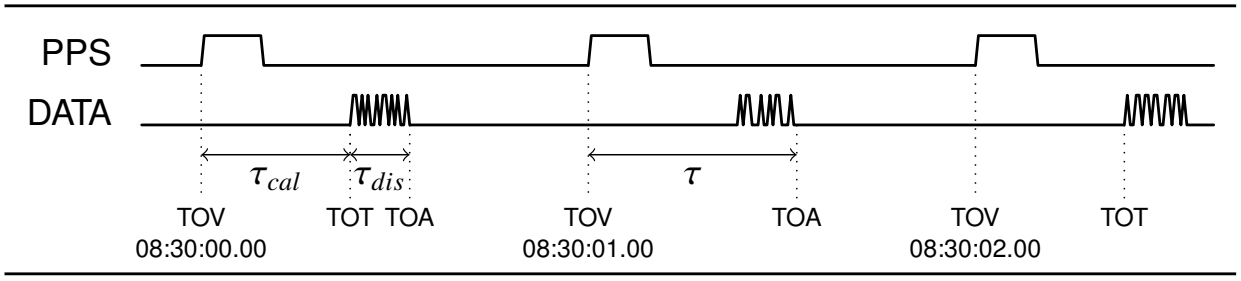

Figure 1: Visualization of PPS and data signal on a time-scale, depicting the time-delay estimation of a GNSS-receiver, see [31].

Fig. 1 shows the relation between when a GNSS measurement is valid, TOV, and when it is received, TOA, where data is sent from the receiver to the user between TOT and TOA. The data is shown for a receiver sample interval of $s_{\text{GNSS}} = 1\ s$. Example time stamps of the TOV values are introduced; the first TOV is registered at UTC 8:30:00, and the second TOV at UTC 8:30:01, with the intermediate TOT and TOA belonging to UTC 8:30:00 but arriving τ_{cal} and τ seconds later.

GNSS receivers usually offer position updates with a rate of 1–10 Hz, generating the need for determining the delay for multiple data packages within one PPS interval. This situation is shown in Fig. 2. When estimating the time delay for a data signal with higher frequency than the PPS signal, the first delay is determined as described in Fig. 1, and the consecutive delays are found as the time between a time shifted PPS signal and TOA times, i.e. the time between $PPS + ns_{\text{GNSS}}$ and the last falling edge of the data packages, where $n = [0, 1, 2, \ldots, s_{\text{GNSS}} - 1]$.

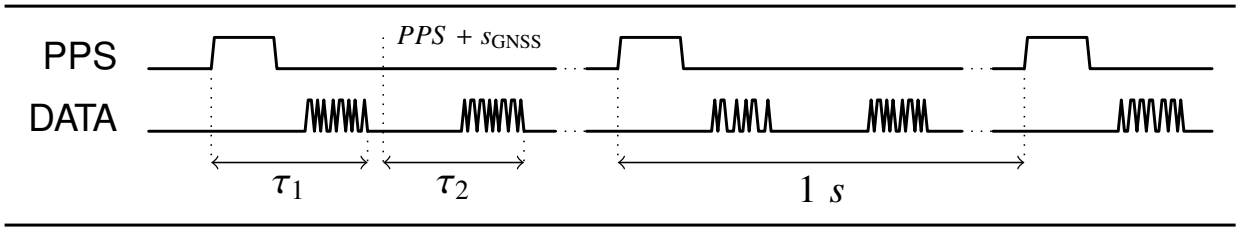

Figure 2: Visualization of time-delay for a GNSS receiver with data frequency higher than 1 Hz.

If the data rate is much higher than the PPS-signal it will become difficult to accurately determine the delays as the relation of a TOV and its corresponding TOA will be obscured: If the data has a much higher frequency than the PPS signal, it becomes uncertain which data package is the first of a PPS interval, as the delay might *displace* a package into the next PPS interval. Having prior knowledge of the approximate delay is essential in determining the maximum data rate the system can support without timing ambiguities.

GNSS receivers can output a multitude of GNSS related data and the magnitude of the time delay will depend on which kind of output is desired. Different delays may be experienced with different data packages, e.g. the ephemeris package containing the satellite trajectories is often shorter than the package containing pseudo-ranges and carrier phase measurements, leading to a shorter time delay. Furthermore, some GNSS packages might change size according to the number of satellites visible in the constellation, which will affect the dissemination delay. Some packages, such as the receiver position packages, have high sample rates ($1 - 10\ Hz$), whereas environmental packages (e.g. the ephemeris packages) are updated on a slower time scale (e.g. $\sim 30\ min$). The proposed method for determining the receiver delay does not depend on the sample rate, and can be used for all types of packages.

2.1. Case Study: Time-Delay Measurement using u-Blox LEA-6T

Let us consider the practical implications of measuring the receiver time delay. One way of visualizing the delay is to use an oscilloscope on the PPS and data signals, allowing for manual measurements of the delay, as shown in

Fig. 1 and 2. Another approach is to use a timer to capture the rising edge of the PPS and the falling edge of the data signal, this can be achieved using a micro-controller.

A test setup including a u-Blox LEA-6T GNSS receiver and a micro-controller is utilized. The advantage of the LEA-6T receiver is that the PPS and data signals are readily available as a digital signal and over a RS-232 connection, respectively. The micro-controller is chosen such that the *input capture* method is available, which time stamp measurements without interrupting the execution when an input is received. Additionally, large counters are available as well as a high-frequency clock to ensure accurate time stamping of TOV, TOT and TOA. Three triggers are used: one for PPS (determining TOV) and two for data signal (determining TOT and TOA), all time stamping in clock cycles, which can be converted to seconds with the known clock frequency.

GNSS measurements are collected using the test-setup with a sample frequency of 5Hz, yielding the results shown in Fig. 3 and Fig. 4. The test is carried out for the raw satellite data including the range and range-rate measurements. This is chosen as worst case as the raw data package is the longest one available on the u-Blox LEA-6T receiver.

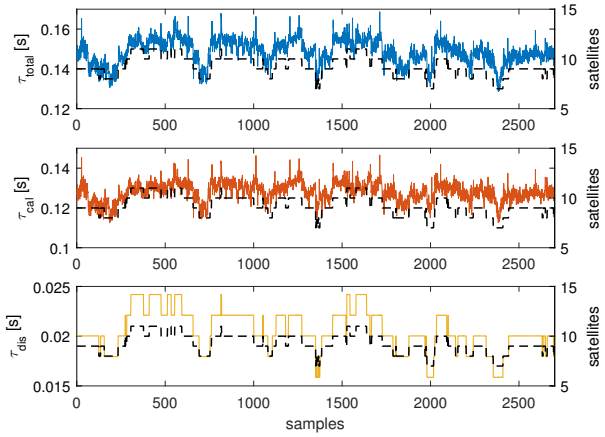

Figure 3: The dissemination (yellow), calculation (red) and total (blue) delay over time, shown with the number of satellites (dashed).

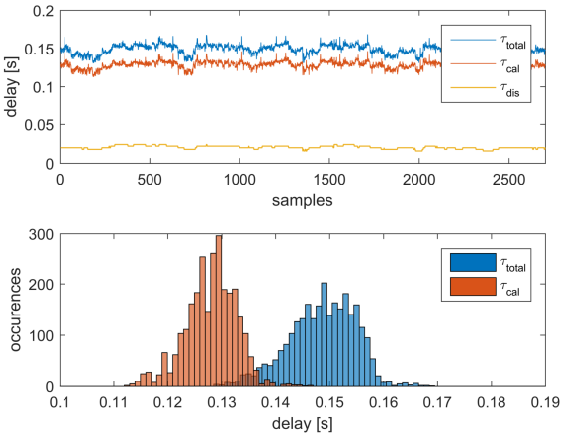

Figure 4: The delays over time and the histogram of calculation (red) and total (blue) delay for range and range-rate data.

The delays determined over time are shown in Fig. 3, where the time delay is seen to be slowly time-varying. It is clear that $\tau_{dis} << \tau_{cal}$ and that there is more variation on the calculation delay than on the dissemination delay. The calculation delay and especially the dissemination delay are seen to be dependent on the number of satellites in the constellation.

The histogram of the observed time delays shown in Fig. 4 conveys that the calculation delay and thereby the total delay are not constant. The mean and standard deviation of the time delays are summaried in Table 1.

Table 1: Characteristics of delay distribution, (unit: seconds).

	τ_{dis}	τ_{cal}	τ_{total}
Mean:	0.0206	0.1281	0.1486
STD:	0.0020	0.0047	0.0062

A time delay of 150 ms will have small impact on e.g. pedestrian applications (position error of < 0.5 m), whereas for cars or UAVs the position error can be several meters (i.e. 5 m error at speeds of 120 km/h).

3. Problem Formulation

The objective is to estimate the current position of a vehicle based on strapdown inertial navigation aided by time-delayed GNSS measurements. The inertial measurements include accelerometer and gyroscope data, integrated with

magnetometer and delayed GNSS data in a loosely coupled nonlinear observer. The GNSS data will be time delayed with τ_p or τ_v seconds, for position and velocity data respectively. For some receivers these delays will be the same, however in the following the general delay will be represented as; $\tau = \max(\tau_p, \tau_v)$.

The position, linear velocity and attitude (PVA) of the vehicle are to be determined. The position, p^e, and linear velocity, v^e, are estimated in the ECEF-frame while the attitude is represented as a unit quaternion, q_b^e, describing the rotation from ECEF- to Body-frame. Furthermore the gyro bias, b^b, is estimated.

The kinematic equations of the vehicle given in [11] and [5] will here be considered in a time-shifted version, where all measurements have been delayed to coincide with the GNSS measurements. The time shifted kinematic equations are:

$$\dot{p}^e(t-\tau) = v^e(t-\tau), \tag{1}$$

$$\dot{v}^e(t-\tau) = -2S\left(\omega_{ie}^e(t-\tau)\right)v^e(t-\tau) + R(q_b^e(t-\tau))f^b(t-\tau) + g^e(p^e(t-\tau)), \tag{2}$$

$$\dot{q}_b^e(t-\tau) = \frac{1}{2}q_b^e(t-\tau)\otimes\bar{\omega}_{ib}^b(t-\tau) - \frac{1}{2}\bar{\omega}_{ie}^e\otimes q_b^e(t-\tau), \tag{3}$$

$$\dot{b}^b(t-\tau) = 0. \tag{4}$$

The specific force of the vehicle is denoted f^b, while the local gravitation vector, $g^e(p^e)$, is assumed known.

The goal of this paper is the design of a loosely coupled nonlinear observer integrating inertial measurements with time delayed GNSS measurements, considering the delay as known such that the delay does not need estimating. Multiple tests in simulation and with experimental data will confirm the observer structure and investigate the impact of a time varying or distributed delay.

3.1. Sensor Configuration

The following measurements are assumed to be available:

- Global position estimate experiencing a time delay, $p^e_{\text{GNSS}}(t-\tau_p) = p^e(t-\tau_p)$, measured using a GNSS receiver.
- Global linear velocity estimates experiencing a time delay, $v^e_{\text{GNSS}}(t-\tau_v) = C_v v^e(t-\tau_v)$, measured by a GNSS receiver.
- Specific force, $f^b(t)$, as measured by the IMU: $f^b_{\text{IMU}}(t) = f^b(t)$.
- Angular velocity, $\omega^b_{ib}(t)$, measured by the IMU, with a bias: $\omega^b_{ib,\text{IMU}}(t) = \omega^b_{ib}(t) + b^b(t)$.
- Magnetometer measurement of the Earth magnetic field measured using a magnetometer, $m^b(t)$.

It is further assumed that the positioning data is available with a sample interval of s_{GNSS} while the inertial and magnetometer measurements are available with a higher frequency $s_{\text{IMU}} > s_{\text{GNSS}}$. The velocity measurements can be a full or partial measurement $v^e_{\text{GNSS}} = C_v v^e$, where the selection matrix C_v may be zero.

4. Nonlinear Observer Design

The proposed observer structure consists of: an attitude estimator, delayed translational motion observer, delayed inertial measurements, and a fast simulator, see Fig. 5. The proposed approach can be generally applied to GNSS/INS integration schemes, and will here be demonstrated on a nonlinear observer. The fast (faster than real-time) simulator is used to estimate the current position and linear velocity from the time-delayed states and a window of IMU data. The attitude observer is developed by Grip et al. [5], and will here be time shifted from t to $t-\tau$ to accommodate for the delayed position measurements by delaying the inertial measurements at the input of the attitude observer. Since the signals are delayed at the input to the observer and therefore affects the entire observer the stability proof can be repeated by shifting the time argument. The origin of the error dynamics of the presented observer structure is therefore semi-global exponential stability. Consequently, the observer will be presented without proof. A similar observer could be used, but the attitude observer from [5] was chosen based on the global stability results. For the alternative implementation proposed in Section 5 it is important that the observer structure is modular.

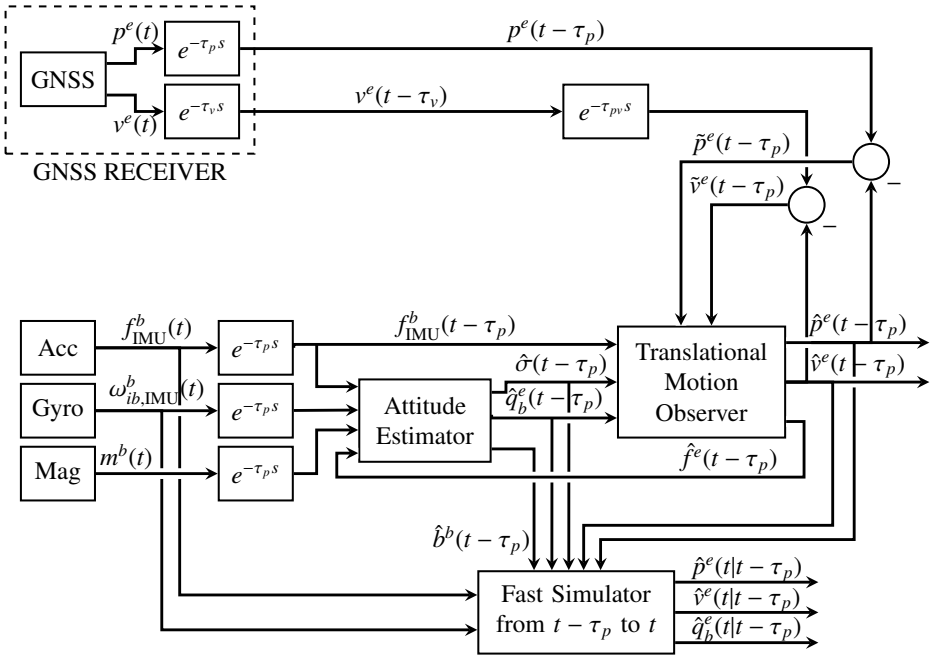

Figure 5: Block diagram structure of the proposed observer design, with; GNSS-receiver, IMU, magnetometer, attitude estimator, time-delayed state observer, and fast simulator.

Even though the GNSS receiver measures both position and velocity, some receivers will have different delays on the two outputs, as they are not subjected to the same computational process. In the following the delayed GNSS measurements will have a distinction between the delay of the position measurement, τ_p, and the velocity measurement, τ_v. The presented approach offers a solution when $\tau_p \geq \tau_v$. In Fig. 5 the linear velocity estimate is delayed to coincide with the measurement, but since it is already delayed with τ_p the additional delay imposed is $\tau_{vp} = \tau_p - \tau_v$. If $\tau_v \geq \tau_p$ the position estimate should be delayed instead of the velocity estimate, and the observer should be delayed with τ_v rather than τ_p as shown here.

4.1. Attitude Estimation

The INS attitude estimator is based on [11] and [5]. The main idea is to estimate the quaternion and gyro bias by using the rotation rate, $\omega^b_{ib,\text{IMU}}$, aided by two non-parallel Body frame vector measurements with known ECEF reference vectors.

The attitude and gyroscope bias are estimated by:

$$\dot{\hat{q}}^e_b(t-\tau) = \frac{1}{2}\hat{q}^e_b(t-\tau) \otimes \left(\bar{\omega}^b_{ib,\text{IMU}}(t-\tau) - \bar{\hat{b}}^b(t-\tau) + \bar{\hat{\sigma}}(t-\tau)\right) - \frac{1}{2}\bar{\omega}^e_{ie} \otimes \hat{q}^e_b(t-\tau), \tag{5}$$

$$\dot{\hat{b}}^b(t-\tau) = \text{Proj}\left(\hat{b}^b(t-\tau), -k_I\hat{\sigma}(t-\tau)\right), \tag{6}$$

where $k_I > 0$ is a constant and $\text{Proj}(\cdot,\cdot)$ denotes the parameter projection where the bias estimate is restricted to a compact set given as a sphere with constant radius M_b, i.e. $\|\hat{b}^b\| \leq M_b$. The injection term, $\hat{\sigma}$, used in (5) and (6) is given as:

$$\hat{\sigma}(t-\tau) := k_1 v^b_1(t-\tau) \times R(\hat{q}^e_b(t-\tau))^T v^e_1(t-\tau) + k_2 v^b_2(t-\tau) \times R(\hat{q}^e_b(t-\tau))^T v^e_2(t-\tau), \tag{7}$$

where the gains k_1 and k_2 satisfy $k_1 \geq k_p$ and $k_2 \geq k_p$ for some sufficiently large positive k_p. The vectors v^b_1 and v^b_2 are two vectors in the Body frame with their corresponding vectors v^e_1 and v^e_2 in the ECEF frame. The vectors can be chosen in various ways. Here they will be considered as:

$$v^b_1 = \frac{f^b_{\text{IMU}}}{\|f^b_{\text{IMU}}\|}, \qquad v^b_2 = \frac{m^b}{\|m^b\|} \times v^b_1, \qquad v^e_1 = \frac{\hat{f}^e}{\|\hat{f}^e\|}, \qquad v^e_2 = \frac{m^e}{\|m^e\|} \times v^e_1, \tag{8}$$

where m^e is the local magnetic field of the Earth and $\hat{f}^e$ is an estimate of the specific force in the ECEF frame, which is provided as described in Section 4.2.

4.2. Translational Motion Observer

The objective of the translational motion observer is to integrate IMU acceleration and GNSS position to produce estimates of position, linear velocity and specific force. Since the GNSS measurements are delayed it is proposed to delay the IMU measurements such that the measurements coincide in time, and estimate the delayed state. The delayed state observer becomes:

$$\dot{\hat{p}}^e(t-\tau_p) = \hat{v}^e(t-\tau_p) + \theta K_{pp}(p^e(t-\tau_p) - \hat{p}^e(t-\tau_p)) + K_{pv}\left(v^e(t-\tau_p) - \hat{v}^e(t-\tau_p)\right), \tag{9}$$

$$\begin{aligned}\dot{\hat{v}}^e(t-\tau_p) = &-2S(\omega_{ie}^e)\hat{v}^e(t-\tau_p) + \hat{f}^e(t-\tau_p) + g^e(\hat{p}^e(t-\tau_p)) + \theta^2 K_{vp}(p^e(t-\tau_p) - \hat{p}^e(t-\tau_p)) \\ &+ \theta K_{vv}\left(v^e(t-\tau_p) - \hat{v}^e(t-\tau_p)\right),\end{aligned} \tag{10}$$

$$\begin{aligned}\dot{\xi}(t-\tau_p) = &-R(\hat{q}_b^e(t-\tau_p))S(\hat{\sigma}(t-\tau_p))f_{\mathrm{IMU}}^b(t-\tau_p) + \theta^3 K_{\xi p}(p^e(t-\tau_p) - \hat{p}^e(t-\tau_p)) \\ &+ \theta^2 K_{\xi v}\left(v^e(t-\tau_p) - \hat{v}^e(t-\tau_p)\right),\end{aligned} \tag{11}$$

$$\hat{f}^e(t-\tau_p) = R(\hat{q}_b^e(t-\tau_p))f_{\mathrm{IMU}}^b(t-\tau_p) + \xi(t-\tau_p), \tag{12}$$

where ξ is an auxiliary state to help in estimating the specific force, $\hat{f}^e$. Here $\theta \geq 1$ is a tuning parameter, and K_{pp}, K_{vp}, $K_{\xi p}$, K_{pv}, K_{vv} and $K_{\xi v}$ are gain matrices chosen to ensure that the error dynamics defined by $\mathcal{A} - \mathcal{K}C$ is Hurwitz, [5]:

$$\mathcal{A} = \begin{bmatrix} 0 & I_3 & 0 \\ 0 & 0 & I_3 \\ 0 & 0 & 0 \end{bmatrix}, \quad \mathcal{K} = \begin{bmatrix} K_{pp} & K_{pv} \\ K_{vp} & K_{vv} \\ K_{\xi p} & K_{\xi p} \end{bmatrix}, \quad C = \begin{bmatrix} I_3 & 0 & 0 \\ 0 & C_v & 0 \end{bmatrix}. \tag{13}$$

The gain matrix $\mathcal{K}$ can be determined in various ways. An advantage of this observer structure is that the gain $\mathcal{K}$ can be chosen constant, as shown in [5], leading to a small computational footprint. Another approach is to solve the discrete time-varying Riccatti equation, thereby computing the gain and covariance matrix similarly to the Kalman filter:

$$P_{k|k} = FP_{k-1|k-1}F^\intercal + Q, \tag{14}$$

$$K_k = P_{k|k-1}C^\intercal\left(CP_{k|k-1}C^\intercal + R\right)^{-1}, \tag{15}$$

$$P_{k|k} = (I - K_kC)\,P_{k|k-1}\,(I - K_kC)^\intercal + K_kRK_k^\intercal, \tag{16}$$

where P, R and Q are the covariance matrices of the estimate, measurements and process noises, respectively. The discretized system matrix, $F = e^{AT}$, where T is the sample time and k is the time index signifying the discrete time update. More details about the discretization and implementation of the nonlinear observer can be found in [32].

4.3. Fast Simulator

The outputs of the time-delayed translational motion observer are the delayed position and linear velocity estimates. In order to get the current position and linear velocity, $\hat{p}^e(t)$ and $\hat{v}^e(t)$, a fast simulator is implemented. The input to the fast simulator is the bias-compensated gyro measurements, as well as the acceleration measured by the IMU, without the gravitational component and rotated to the ECEF frame, $u(t) = a^e(t) = R(\hat{q}_b^e(t))f_{\mathrm{IMU}}^b - g^e(\hat{p}^e(t))$. Moreover, the fast simulator is implemented as,

$$\hat{v}^e(t|t-\tau_p) = \hat{v}^e(t-\tau_p) + \int_{t-\tau_p}^{t} u(r)dr, \tag{17}$$

$$\hat{p}^e(t|t-\tau_p) = \hat{p}^e(t-\tau_p) + \tau_p\hat{v}^e(t-\tau_p) + \int_{t-\tau_p}^{t}\int_{t-\tau_p}^{s} u(r)drds, \tag{18}$$

$$\dot{\hat{q}}_b^e(t-\tau_p) = \frac{1}{2}\hat{q}_b^e(t-\tau_p) \otimes \left(\bar{\omega}_{ib}^b(t-\tau_p) - \bar{\hat{b}}^b(t-\tau_p) + \bar{\hat{\sigma}}(t-\tau_p)\right) - \frac{1}{2}\bar{\omega}_{ie}^e \otimes \hat{q}_b^e(t-\tau_p), \tag{19}$$

where $\hat{p}^e(t-\tau)$ and $\hat{v}^e(t-\tau)$ are estimated by the translational motion observer.

The fast simulator can be implemented offline where the attitude estimates of (5) can be saved in a buffer, avoiding the need for (19), or online where the attitude must be estimated in the fast simulator. Used online the fast simulator must have a data buffer for storing measurements for use in the integrations. The integral part of (17) can be implemented as a for-loop and can be used in the double integral of (18) to save computational effort. The frequency of the fast simulator is the runtime frequency of the implementation platform, with the minimal requirement of being faster than the IMU sample rate. To further save computations the latest value of $u(t)$ can be determined and appended to an array. The integrals can then be calculated by summing the elements in the array over the relevant time horizon. This solution uses a running horizon method and will limit the computational load as only one u is determined every iteration.

5. Alternative Implementation

An alternative implementation of the proposed observer can be designed by changing the placement of the delay that ensures the translational motion observer use coinciding data. In the proposed observer structure the delay was placed before the attitude estimator while in the alternative implementation, shown in Fig. 6, the delay is implemented after the attitude estimator. The attitude estimator thereby supply the present attitude estimate, negating the need for estimating the attitude in the fast simulator.

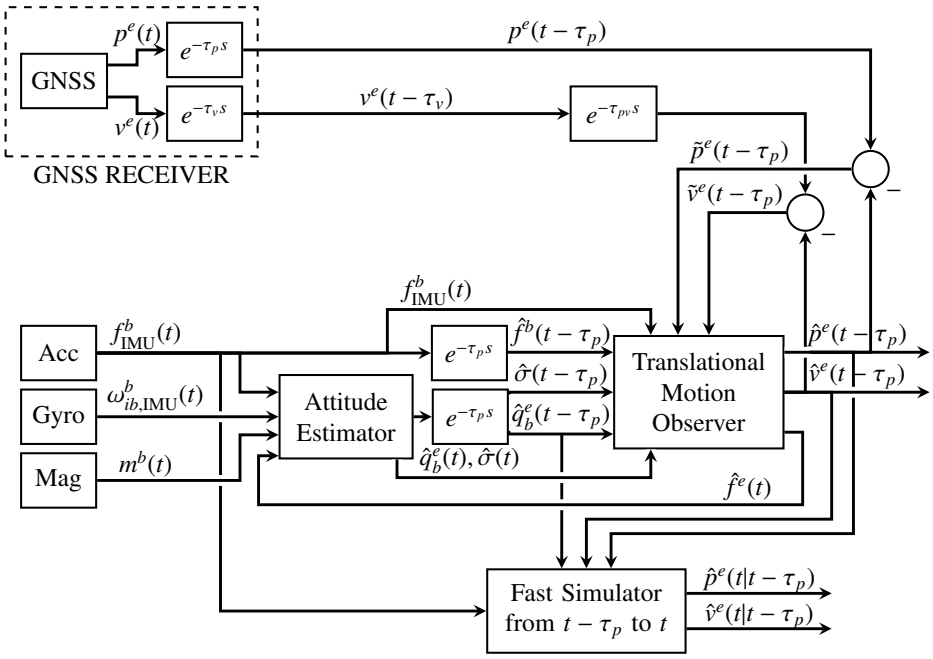

Figure 6: Block diagram structure of the alternative implementation, with; GNSS receiver, IMU, magnetometer, attitude estimator, time-delayed translational motion observer, and fast simulator.

The fast simulator for determining the present position and velocity is identical to the fast simulator in the observer structure proposed in Section 4, and depends on; $\hat{v}^e(t-\tau_p)$, $\hat{p}^e(t-\tau_p)$, $f^b_{\text{IMU}}(t)$, and $\hat{q}^e_b(t-\tau_p)$. However, it is no longer necessary to estimate the present attitude.

The alternative implementation can be applied to any other modular GNSS/INS integration scheme where the attitude and translational motion observers are separated. The alternative implementation approach alters the observer structure and the stability proof is no longer valid. Here the alternative implementation is stated without stability proof. There might exist an observer where the stability is not violated by the structure of the alternative implementation. To the best of the authors knowledge there is no modular observer where the stability results account for a delay in the interconnection.

The delayed specific force estimate from the translational motion observer is used in the attitude observer. An additional fast simulator could be introduced to integrate the ξ state over the time delay horizon. However, to save computations an approximation is introduced such that ξ and $\hat{f}^e$ are estimated as:

$$\dot{\xi}(t) = -R(\hat{q}_b^e(t))S(\hat{\sigma}(t))f_{\text{IMU}}^b(t) + \theta^3 K_{\xi p}(p^e(t-\tau_p) - \hat{p}^e(t-\tau_p)) + \theta^2 K_{\xi v}(v^e(t-\tau_p) - \hat{v}^e(t-\tau_p)), \tag{20}$$

$$\hat{f}^e(t) = R(\hat{q}_b^e(t))f_{\text{IMU}}^b(t) + \xi(t), \tag{21}$$

The approximation only lies in estimation of $\xi(t)$, whereas (21) is identical to (12) with the time shift from $t - \tau_p$ to t.

5.1. Computational Load

The computational loads of the proposed observer and the alternative implementation are compared by counting the average number of multiplications and additions required. The comparison is shown in Table 2, where the attitude estimator operates at IMU frequency, 500 Hz, and the TMO gain computation runs at GNSS receiver frequency, 5 Hz. Furthermore, the time delay is considered constant with a ratio to the IMU frequency of 10, such that the integrals in the fast simulators are determined over 10 elements. The proposed observer is denoted NLO, while the alternative implementation is NLO-ALT. The observers are compared to a fixed TMO gain implementation of the proposed observer, here denoted NLO-FIX, and the uncompensated observer, denoted NLO-UNC, which does not take the time delay into account.

Table 2: Numerical comparison of computational load. The values are average number of arithmetic operations per second.

	NLO-UNC		**NLO**		**NLO-FIX**		**NLO-ALT**	
	Mult.	Add.	Mult.	Add.	Mult.	Add.	Mult.	Add.
Attitude estimation (500 Hz)	66500	58000	66500	58000	66500	58000	66500	58000
TMO prediction (500 Hz)	441500	399000	441500	399000	77000	70500	441500	399000
TMO correction (5 Hz)	24840	14745	24840	14745	9225	300	24840	14745
TMO gain computation (5 Hz)	8910	7740	8910	7740	–	–	8910	7740
Fast simulator (500 Hz)	–	–	44000	82000	44000	82000	24000	62000
Total	541750	479485	585750	561485	196725	210800	565750	541485
Ratio	1.00	1.00	1.08	1.17	0.36	0.44	1.04	1.13

The computational load of the NLO-UNC observer is used as reference when determining the change in computational load of the proposed observers. The rations between the computational load of the observers and the NLO-UNC are listed in the table. The fixed gain method offers a significant reduction in computational load despite inclusion of the fast simulator. The load of the proposed NLO is larger than the uncompensated observer due to the addition of the fast simulator, while the alternative implementation offers a reduction in load compared to the NLO, due to the removal of the attitude estimate in the fast simulator.

6. Simulation Study

The implementation and effect of the proposed observer structures are verified in simulation using the unmanned aerial vehicle (UAV) model of Beard and McLain [33], estimating UAV position in NED, linear velocity, attitude, acceleration, and angular velocity of the Aerosonde UAV.

The simulation setup will be the same for the three tests, with the reference position being a circular path with diameter of 1300 m. The simulated GNSS data is supplied with a frequency of 5 Hz with added Gaussian white noise. The standard deviation of the position measurements is 1 m, while the velocity measurements has a standard deviation of 0.01 m/s. These standard deviations are reasonably realistic with differential corrections chosen to better visualize the conceptual difference in performance between the observers. The inertial measurements will be supplied with a frequency of 500 Hz and Gaussian white noise comparable to the ADIS 16488 IMU (accelerometer: $1.5 \cdot 10^{-3}$ g, magnetometer: $0.45 \cdot 10^{-7}$ T, gyroscope: 0.0028 rad/s).

The observer parameters are chosen as; $M_b = 0.0087$, $k_1 = 1.8$, $k_2 = 1.2$, $k_I = 0.004$, and $\theta = 1$. The parameters are tuned by the guidelines presented in the stability proof in Grip et al. [5] where $\theta \geq 1$, and $k_* \geq k_p > 0$ with M_b being sufficiently large. Futher suggestions for tuning can be found in Bryne et al. [32]. The observer gain matrices are found by solving the discrete time-varying Riccati equation, where the covariance matrices are selected as: $R = \text{blockdiag}(I_3, 0.01I_3)$, and $Q = \text{blockdiag}(0I_3, 1 \cdot 10^{-3}I_3, 2.5 \cdot 10^{-4}I_3)$. The observers are implemented using a corrector-predictor representation of the discretized system [34] with two time scales: GNSS data and the time-delayed IMU data.

The observers robustness towards errors in the time-delay estimate is tested by distinguishing between the delay introduced by the GNSS receiver and the implemented delays, where the GNSS delay (τ_p and τ_v) is the actual time delay experienced in the GNSS receiver, whereas the implementation delay ($\tau_{p,imp}$ and $\tau_{v,imp}$) is the delay assumed in the observer. A perfect correspondence between the two delays gives the best result, however the GNSS delay might vary over time making a constant implementation delay inaccurate.

Several simulations are carried out comparing the proposed observer and the alternative implementation with the traditional observer structure without time delay compensation: I) the time delay is constant $\tau_p = \tau_v = \tau_{p,imp} = \tau_{v,imp} = 150\ ms$, II) an inaccurate time-delay estimation is considered, where the observed time delay does not match the time delay used in the observer implementation, and III) a normal distributed observed delay while the implemented delay is fixed at the mean value.

6.1. Attitude and Position Representation

To a user the representation of PVA in the ECEF frame is of little direct use. A more intuitive reference frame is e.g. a NED-frame where the user can compare a change in position or velocity to a local point and where the heading can be intuitively verified by comparison to North. Comparing the attitude of a vehicle is more intuitive in a local frame than a global, why the attitude will be converted to a rotation between the Body and NED frames.

The attitude estimates of the observer represent the rotation from the Body frame to the ECEF frame, which can be decomposed into two parts; Body to NED, $\hat{q}_b^n$, and NED to ECEF, $\hat{q}_n^e$. In other words the attitude from Body to NED can be estimated from the observer attitude estimate, $\hat{q}_b^e$, and the rotation between NED and ECEF. Estimating the rotation between the NED and ECEF coordinate systems is determined from the position in latitude, μ, and longitude, l, as $\hat{q}_e^n = \hat{q}_\mu \otimes \hat{q}_\mu$, where $\hat{q}_l = \left[\cos\left(\hat{l}/2\right); 0; 0; -\sin\left(\hat{l}/2\right)\right]$ and $\hat{q}_\mu = [\cos\left((\hat{\mu} + \pi/2)/2\right); 0; \sin\left((\hat{\mu} + \pi/2)/2\right); 0]$. Then finally the attitude from Body to NED can be determined as: $\hat{q}_b^n = \hat{q}_e^n \otimes \hat{q}_b^e$.

6.2. Test I: Simulation with $\tau = 150\ ms$

The proposed observer and the alternative implementation are simulated with a time delay of $\tau = 150\ ms$, matching the delay found from experimental data in Section 2. The experienced and implemented delay coincide in this test; $\tau_* = \tau_{*,imp}$. The true position of the UAV is known, and the position estimation error is shown in Fig. 7. The position error of three observers are shown: a) the proposed observer, b) the alternative implementation, and c) an observer without delay compensation.

The observer without delay compensation is seen to introduce a sinusoid error characteristic, whereas the proposed observer and alternative implementation have estimation errors concentrated around zero. It is evident that taking the time delay of the GNSS receiver increases performance of the observer structure.

The root-mean-square (RMS) and standard deviation (STD) of the estimation error is summaries in Table 3. Since the GNSS receiver position measurements have a standard deviation of 1 m the delay compensated observer improves the accuracy compared to using only GNSS measurements, while the uncompensated observer leads to higher standard deviation.

6.3. Test II: Simulations with Inaccurate Time Delay

In order to test the performance of the proposed observer structures when magnitude of the time delay is not precisely known, a test is carried out where the implemented delay is larger than the experienced delay, i.e $\tau_{*,imp} = 1.5\tau_* = 225\ ms$. The position estimation errors are shown in Fig. 8.

Comparing the position errors in Fig. 7 with Fig. 8 there is no difference in the error of the observer without time-delay compensation (as expected), however the error from the proposed observer and the alternative implementation

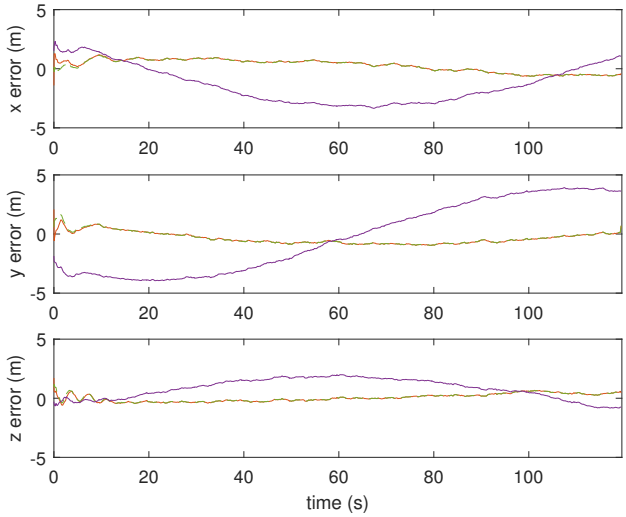

Figure 7: Position estimation error the proposed observer structure (red), the alternative implementation (green) and the observer without time-delay compensation (purple).

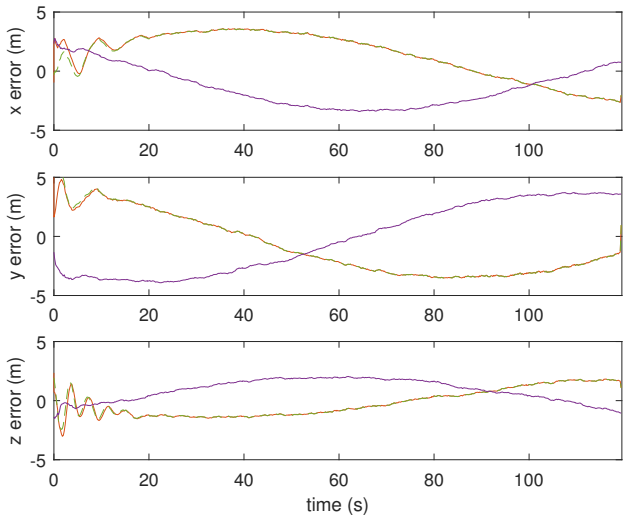

Figure 8: Position estimation error the proposed observer structure (red), the alternative implementation (green) and the observer without time-delay compensation (purple).

have grown to a magnitude that is comparable to the error of the uncompensated observer. While a good estimate of the receiver delay is desired the simulation show that the estimate can be a factor of 1.5 larger than the true delay magnitude, without the uncompensated observer becoming a better candidate for position estimation. The results are summarised in Table 3.

6.4. Test III: Simulations with Distributed Delay

To investigate the performance of the observer structures with regards to a non-constant time delay, the experienced delay is introduced as a time-varying delay with a mean of 0.150 s and normal distribution with a standard deviation of 0.0075 s, while the implemented delay, $\tau_{p,imp}$ is fixed at the mean value of the distribution. This case study will resemble the tendency of the experienced delay, while opting for the straightforward implementation of a constant delay in the observer structure.

The estimation errors can be seen in Fig. 9, closely resembling the performance shown in Fig. 9 for a constant and perfectly known delay.

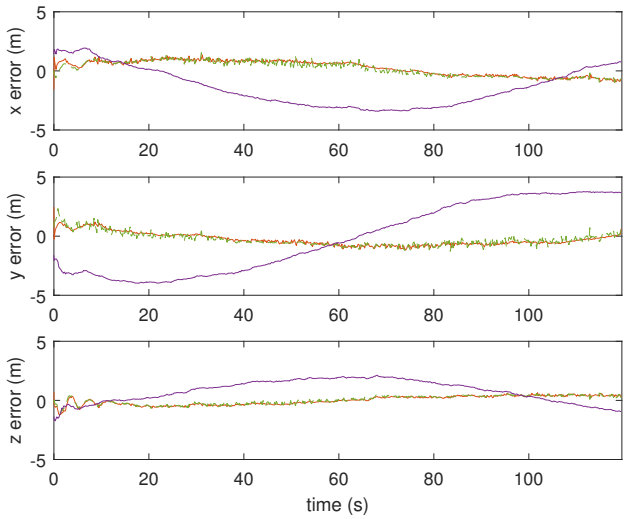

Figure 9: Position estimation error the proposed observer structure (red), the alternative implementation (green) and the observer without time-delay compensation (purple).

The estimation error of the proposed observer and the alternative implementation is concentrated around zero, with clear advantages compared to the observer without delay compensation. The results are summaries in Table 3.

Table 3: Simulation results, summarising the RMS and STD of position error signals of considered observer structures. Note that the simulated GNSS position noise STD is 1 m.

		RMS			STD		
		x	y	z	x	y	z
Test I	Proposed Observer	0.6880	0.5680	0.3232	0.6170	0.4814	0.3112
	Alternative Implementation	0.6633	0.5842	0.3173	0.6013	0.5085	0.3018
	Uncompensated Observer	2.0926	2.9825	1.2362	1.6391	2.9748	0.8867
Test II	Proposed Observer	2.3901	2.5953	1.1720	1.9358	2.4460	1.1522
	Alternative Implementation	2.3595	2.6617	1.1557	1.9308	2.5284	1.1386
	Uncompensated Observer	2.1297	2.8880	1.2623	1.6464	2.8778	0.9132
Test III	Proposed Observer	0.6851	0.6069	0.3776	0.6305	0.5379	0.3778
	Alternative Implementation	0.6592	0.6197	0.3661	0.6290	0.5597	0.3652
	Uncompensated Observer	2.1244	2.9238	1.2156	1.6158	2.9181	0.9230

From the table it is clear that the proposed observer and the alternative implementation have similar performance, throughout the test cases, while performing better than the observer without delay compensation. Furthermore, the performances in test I and test II are very similar, suggesting that when the receiver delay has a small standard deviation the implemented delay can be kept constant. The average delay of the receiver can be determined prior to implementation, and as test II showed, does not have to perfectly correspond to the experienced delays throughout the test. Moreover, the average delay of the receiver can be determined prior to use, possibly negating the need for online delay estimation for this specific receiver and thereby the use of the PPS signal in the on-board autopilot. In general it must be expected that other receivers and configurations might show larger variations in the time delay estimation.

7. Experimental Results

This section describes the data acquisition and experimental results achieved with the introduced observers. A payload consisting of an ADIS 16488 IMU (at 1230 Hz), a u-Blox LEA-M8T GNSS receiver (at 5 Hz) and custom hardware for accurately time stamping the measurements with GPS clock was used for data acquisition. The proposed observers were implemented for post-processing of the acquired measurements. Both GNSS position and velocity measurements are used for estimation. The datasets were collected during flights with a GA Slingsby T67C, small manned aircraft, see Fig. 10, operated at an airfield in Prague.

Figure 10: Aircraft (GA Slingsby T67C)

The payload was mounted behind the passenger seat, powered by a car battery, with the GNSS antenna mounted on the inside of the transparent cover, directly above the payload to minimize the lever arm. The aircraft is highly manoeuvrable with maximum speed of approximately 280 km/h.

The trajectory reference was determined as a Real-Time-Kinematic (RTK) solution using dual frequency receiver onboard the aircraft with corrections from a local base station. The RTK solution, computed by the open source RTKLIB, exploiting carrier-phase measurements, provides more accurate data than the single-receiver code-based GPS solution, with three quality categories; single (the solution is comparable with the single receiver solution), float (relative positioning but unresolved ambiguities), and fixed (relative positioning with resolved ambiguities). The flight had predominant (over 90% of the time) "fixed" quality indicating a highly accurate reference. The remaining time the reference had "float" quality were the differential corrections are used, without the resolution of the integer ambiguity.

When comparing the observer position estimates with the RTK solution, the position estimates are down sampled to match the frequency of the RTK solution.

The receiver delay was measured in real time throughout the flight. The time delay was slowly time varying over time, see Fig. 11, with distribution as shown in Fig. 12. The receiver used in the experimental verification is a newer version compared to the receiver presented in Section 2.1, which might account for the smaller magnitude in total delay. The mean of the distribution is 0.0505 s with standard deviation 0.0020 s. The error introduced at maximum speed of the aircraft will be approximately 4 m.

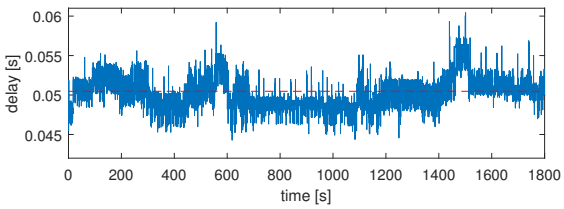

Figure 11: Total receiver delay (blue) with depicted average (red).

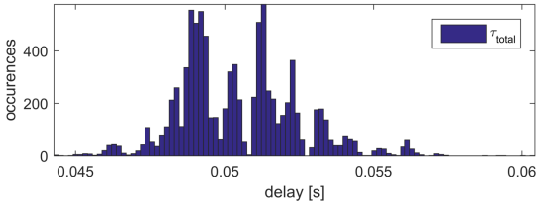

Figure 12: Histogram of total receiver delay.

When implementing the proposed observer structures the receiver delay is represented as an integer number of IMU samples. As the average receiver delay is equivalent to 62 IMU samples the delay is considered sufficiently well represented.

The observer parameters are chosen as; $M_b = 0.0087$, $k_1 = 0.8$, $k_2 = 0.2$, $k_I = 0.004$, and $\theta = 1$. The gain matrices of the TMO are determined by solving the discrete Ricatti equation with the noise covariance matrices; $R = \text{blockdiag}(14.4I_3, 1{\cdot}10^{-4}I_3)$, and $Q = \text{blockdiag}(0I_3, 0.096I_3, 2.5{\cdot}10^{-2}I_3)$. In the injection term for the attitude observer the magnetometer measurements are exchanged for velocity estimates making; $v_2^b = [1; 0; 0]$ and $v_2^e = \hat{v}^e / \|\hat{v}^e\|_2$.

In the following two tests are presented, both with the experienced delay as the actual distributed delay as shown in Fig. 11 and Fig. 12, while; 1) the implemented delay is constant at the average value, and 2) the implemented delay is follows the actual delay. In both test scenarios the velocity delay will be considered the same as the position delay, $\tau_p = \tau_v$, since the information package used from the receiver included both position and velocity measurements. Three observers will be considered, as in the simulation study; a) the proposed observer, b) the alternative implementation, and c) the uncompensated observer. The results of the observers will be summarised in Table 4, where they are compared using the RMS and STD values using the RTK solution as reference.

The flight trajectory is shown in Fig. 13 covering an area of over 120 km^2 with a flight duration of more than 25 *min*. Certain points of interest have been marked during the flight, where; ① denotes the take off, ② marks a sharp turn with small radius and high roll angle, ③ denotes a stall where the plane first climbed in altitude and then went into stall, and ④ denotes the second stall, where the plane experience accelerations from approximately 0.5 g to 2.1 g over a short time period, during the climb following the stall. These points of interest have been marked on the figures depicting the results for ease of comparison between the trajectory and the signals of interest.

7.1. Test 1: Average Delay

The implemented delay is considered constant and fixed at the average of the actual experience delay, i.e. $\tau_p = \tau_v = \tau_{p,imp} = \tau_{v,imp} = 0.0505$ *s*. The estimated position of the three observers are compared with the reference and the error in ECEF-frame can be seen in Fig. 14.

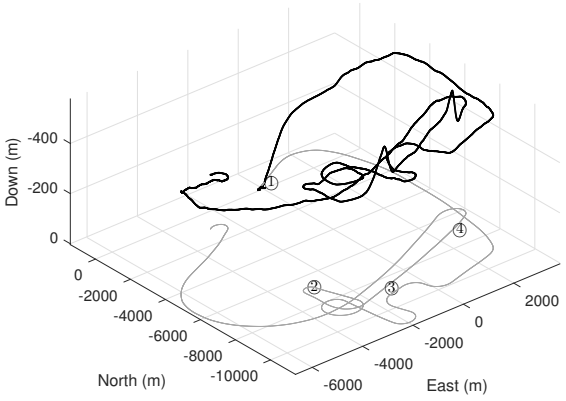

Figure 13: Measured (black) and ground track (gray) trajectory of the aircraft seen in NED frame.

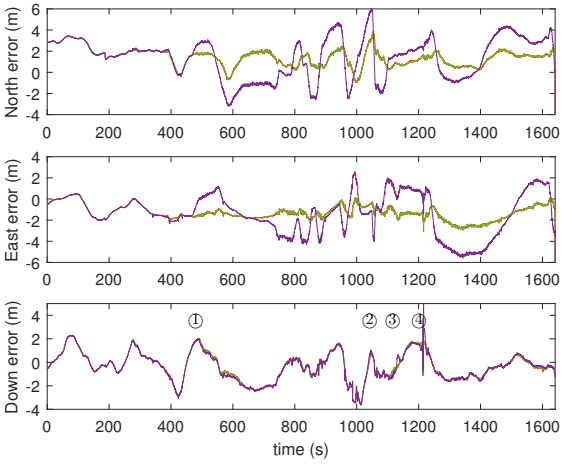

Figure 14: Position error the proposed observer structure (red), the alternative implementation (green) and the observer without time-delay compensation (purple).

During taxiing on the runway, prior to take-off, the position errors of the three observers have comparable magnitude. However after take-off when the aircraft moves with higher speeds than during taxiing the difference between the uncompensated observer and the proposed observer is clear, with the proposed observer structure having smaller error magnitude. There is little difference in the vertical component (as the vertical velocity is small), whereas there is a significant improvement in the North and East components, compared to using the proposed observer instead of the uncompensated observer. The difference between the proposed observer and the alternative implementation is almost indistinguishable. During the sharp turn at ②, which is predominantly in the North direction, the error of the proposed

observer is seen to have a smaller magnitude than the uncompensated observer, as expected due to the high velocity. During the two stall manoeuvres the proposed observer also has better performance than the uncompensated observer.

7.2. Test 2: Actual Delay

The actual time-varying receiver delay is considered for the implemented delay. The position error of the observers are very similar to the once presented in Test 1, as is the case for the attitude and gyro bias estimates shown in Fig. 15 and Fig. 16.

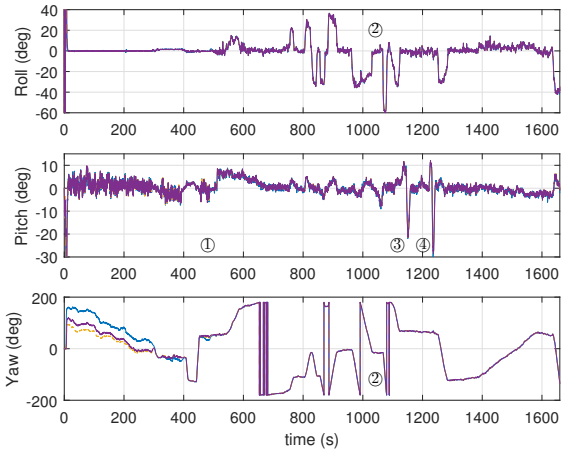

Figure 15: Attitude estimates of the proposed observer structure (red), the alternative implementation (green) and the observer without time-delay compensation (purple).

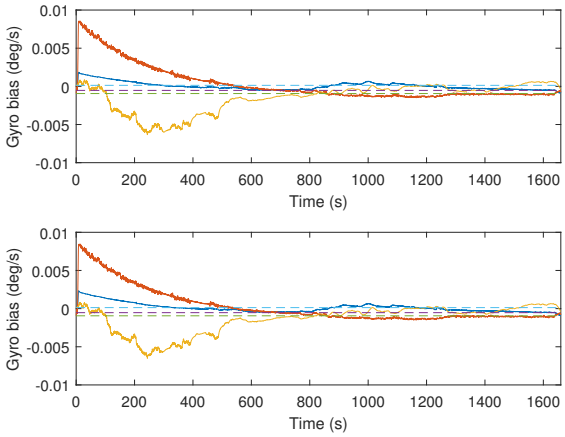

Figure 16: Gyro biases (solid) and biases determined at standstill (dashed) of the proposed observer (top) and alternative implementation (bottom).

The estimated attitude is seen to be very similar for the three observers, with only small differences during the flight. Similarly, the difference in determined gyro biases of the proposed observer and the alternative implementation very small, with convergence towards the biases determined at standstill. The roll angle is seen to be large during the sharp turn, while the pitch is small throughout the flight except for during take-off and the two stall manoeuvres.

Table 4: Summary on RMS and STD of error signals of the uncompensated and proposed, and alternative observers for the test scenarios.

		RMS			STD		
		North	East	Down	North	East	Down
Test 1	Proposed Observer	1.6782	1.4594	1.2368	0.8384	0.6990	1.1891
	Alternative Implementation	1.6788	1.4596	1.2369	0.8391	0.6996	1.1893
	Uncompensated Observer	2.3768	2.3089	1.2501	1.9057	1.8588	1.2010
Test 2	Proposed Observer	1.6710	1.4363	1.2370	0.8319	0.6727	1.1891
	Alternative Implementation	1.6737	1.4392	1.2371	0.8356	0.6781	1.1893
	Uncompensated Observer	2.3768	2.3089	1.2501	1.9057	1.8588	1.2010

From the summarised results in Table 4, it is clear that the proposed observer and the alternative implementation have similar performance, both being superior to the uncompensated observer. The RMS of the error signal is decreased with over 30% in the x and y direction by using the proposed observer structure (or the alternative implementation) compared to the traditional observer structure. The difference between considering the receiver delay constant (shown in Test 1) or time-varying (shown in Test 2) is small. It can be concluded that the proposed observer works well on highly accelerated vehicles experiencing fast dynamic manoeuvres.

8. Concluding Remarks

Nonlinear integration of INS and GNSS have been investigated where the GNSS measurements are delayed due to computational time in the receiver and data communication between receiver and the navigation computer. Initially the delay was investigated and a method for determining the magnitude of the delay was proposed.

An observer structure for compensating the time delay was introduced based on a uniformly semiglobally exponentially stable nonlinear observer. The proposed observer structure includes delaying the inertial and magnetometer measurements to coincide with the GNSS measurements, estimating position, linear velocity, attitude and IMU bias as delayed states, while a faster than real-time simulator supplies current estimates based on the delayed states and current inertial measurements.

Additionally, an alternative implementation was proposed where the current attitude is estimated with the delayed position and velocity. This approach offers a reduction in computational load as the fast simulator does not need to determine the attitude.

The two observer structures was compared to the uncompensated observer structure, where the time delay is not taken into account, through simulations and experimental data from a small manned aircraft. A significant improvement was evident using the proposed observer structures compared to the uncompensated observer.

Acknowledgments

This work was supported by the Norwegian Research Council (projects no. 221666 and 223254) through the Centre of Autonomous Marine Operations and Systems at the Norwegian University of Science and Technology.
The authors would like to thank Jan Roháč and Martin Šipoš, at Czech Technical University in Prague, Faculty of Electrical Engineering, Dept. of Measurement, Czech Republic, for cooperation with the experimental verification. Significant contributions to the construction of the payload was made by the rest of the team at NTNU, in particular Sigurd Albrektsen.

References

[1] Mohinder S. Grewal, Lawrence R. Weill, and Angus P. Andrews. *Global Positioning Systems, Inertial navigation, and Integration*. John Wiley & Sons, Ltd, 2007.

[2] Minh-Duc Hua. Attitude Estimation for Accelerated Vehicles using GPS/INS Measurements. *Control Engineering Practice*, 18:723–732, 2010.

[3] B. Vik and Thor I. Fossen. A Nonlinear Observer for GPS and INS Integration. *Proc. Conference on Decision and Control*, Vol. 3:2956–2961, 2001.

[4] Håvard Fjær Grip, Thor I. Fossen, Tor A. Johansen, and Ali Saberi. Globally Exponentially Stable Attitude and Gyro Bias Estimation with Application to GNSS/INS Integration. *Automatica*, 51:158–166, 2015.

[5] Håvard Fjær Grip, Thor I. Fossen, Tor Arne Johansen, and Ali Saberi. Nonlinear Observer for GNSS-Aided Inertial Navigation with Quaternion-Based Attitude Estimation. *American Control Conference*, -:272–279, 2013.

[6] Robert Mahony, Tarek Hamel, and Jean-Michel Pflimlin. Nonlinear Complementary Filters on the Special Orthogonal Group. *IEEE Transactions on Automatic Control*, 53, No 5:1203–1218, 2008.

[7] T. A. Johansen, J. M. Hansen, and T. I. Fossen. Nonlinear Observer for Tightly Integrated Inertial Navigation Aided by Pseudo-Range Measurements. *ASME J. Dynamic Systems, Measurement and Control*, 2016.

[8] Andrew Roberts and Abdelhamid Tayebi. On the Attitude Estimation of Accelerating Rigid-Bodies Using GPS and IMU Measurements. *50th IEEE Conference on Decision and Control, European Control Conference (CDC-ECC)*, -:8088–8093, 2011.

[9] Minh-Duc Hua, Guillaume Ducard, Tarek Hamel, Robert Mahony, and Konrad Rudin. Implementation of a Nonlinear Attitude Estimator for Aerial Robotic Vehicles. *IEEE Transactions on Control Systems Technology*, 22, No 1.:201–213, 2014.

[10] Derek B. Kingston and Randal W. Beard. Real-Time Attitude and Position Estimation for Small UAVs Using Low-Cost Sensors. *American Institute of Aeronautics and Astronautics, "Unmanned Unlimited"*, -:1–9, 2004.

[11] Håvard Fjær Grip, Thor I. Fossen, Tor Arne Johansen, and Ali Saberi. Attitude Estimation Using Biased Gyro and Vector Measurements With Time-Varying Reference Vectors. *IEEE Transactions on Automatic Control*, 57:1332–1338, 2012.

[12] I. Skog and P. Händel. Effects of time synchronization errors in GNSS-aided INS. In *Position, Location and Navigation Symposium, 2008 IEEE/ION*, pages 82–88, May 2008.

[13] Giovanni Jacovitti and Gaetano Scarano. Discrete Time Techniques for Time Delay Estimation. *IEEE Transactions on Signal Processing*, 41:525–533, 1993.

[14] P. D. Solomon, J. Wang, and C. Rizos. Latency Determination and Compensation in Real-Time GNSS/INS Integrated Navigation Systems. *International Archives of the Photogrammetry, Remote Sensing and Spatial Information Sciences*, XXXVIII-1/C22:–, 2011.

[15] Tobias Raff and Frank Allgöwer. An EKF-Based Observer For Nonlinear Time-Delay Systems. *American Control Conference*, -:4, 2006.

[16] Isaac Skog and Peter Händel. Time Synchronization Errors in Loosely Coupled GPS-Aided Inertial Navigation Systems. *IEEE Transactions on Intelligent Transportation Systems*, 12:1014–1023, 2011.
[17] Mogens Blanke. Fault-tolerant and Diagnostic Methods for Navigation. *International Conference on Marine Engineering Systems (ICMES)*, pages 1–6, 2003.
[18] Mogens Blanke. Fault-tolerant Sensor Fusion for Mairne Navigation. *IFAC Conference on Maneuvering and Control of Marine Craft*, pages 1–6, 2006.
[19] Antonis Papachristodoulou, Matthew Peet, and Sanjay Lall. Constructing Lyapunov-Krasovskii Functionals For Linear Time Delay Systems. *American Control Conference*, 4:2845–2850, 2005.
[20] K. Gu and S-I Niculescu. Advanced Topics in Control Systems Theory. *Chapter 4 in Lecture Notes in Control and Information Science (A. Loria, F. Lamnabhi-Lagarrigue, E. Panteley)*, 328:139–170, 2006.
[21] Pedro Albertos and Pedro Garcia. Predictor-observer-based control of systems with multiple input/output delays. *Journal of Process Control*, 22:1350–1357, 2012.
[22] Amit Ailon and Shai Arogeti. Study on the effects of time-delay on quadrotor-type helicopter dynamics. *Mediterranean Conference on Control and Automation (MED)*, -:305–310, 2014.
[23] Stefano Battilotti. Nonlinear Predictors for Systems with Bounded Trajectories and Delayed Measurements. *Automatica*, 59:127–138, 2015.
[24] Tarek Ahmed-Ali, Iasson Karafyllis, and Françoise Lamnabhi-Lagarrigue. Global Exponential Sampled-Data Observers for Nonlinear Systems with Delay Measurements. *Systems and Control Letters*, Vol. 62:539–549, 2013.
[25] Corentin Briat. *Linear Parameter-Varying and Time-Delay Systems - Analysis, Observation, Filtering and Control*. Springer, 2014.
[26] Emilia Fridman. *Introduction to Time-Delay Systems - Analysis and Control*. Springer, 2014.
[27] Alireza Khosravian, Jochen Trumpf, Robert Mahony, and Tarek Hamel. Velocity Aided Attitude Estimation on SO(3) with Sensor Delay. *IEEE Conference on Decision and Control*, 14:114–120, 2014.
[28] Alireza Khosravian, Jochen Trumpf, Robert Mahony, and Tarek Hamel. Recursive Attitude Estimation in the Presence of Multi-rate and Multi-delay Vector Measurements. *American Control Conference*, -:–, 2015.
[29] Alireza Khosravian, Jochen Trumpf, Robert Mahony, and Christian Lageman. Observers for Invariant Systems on Lie Groups with Biased Input Measurements and Homogeneous Outputs. *Automatica*, -:–, 2015.
[30] Marco Siccardi, Daniele Rovera, and Stefania Romisch. Delay Measurements of PPS Signals in Timing Systems. *Frequency Control Symposium*, 2016.
[31] u Blox. Data sheet - LEA-6 Receiver Description - Including Protocol Specification, `https://www.u-blox.com/images/downloads/Product_Docs/u-blox6_ReceiverDescriptionProtocolSpec_%28GPS.G6-SW-10018%29.pdf`. Technical report, u-Blox, 2011.
[32] T. H. Bryne, J. M. Hansen, R. H. Rogne, N. Sokolova, T. I. Fossen, and T. A. Johansen. Nonlinear Observers for Integrated INS/GNSS Navigation - Implementation Aspects. *IEEE Control Systems Magazine*, 2016.
[33] Randal W. Beard and Timothy W. McLain. *Small Unmanned Aircraft - Theory and Practice*. Princeton University Press, 2012.
[34] Thor I. Fossen. *Handbook of Marine Craft Hydrodynamics and Motion Control*. John Wiley & Sons, Ltd, 2011.